ADVANCED MATERIALS INTERFACES

www.advmatinterfaces.de

# Controlling Interfacial Properties of Lithium-Ion Battery Cathodes with Alkylphosphonate Self-Assembled Monolayers

*Bruno G. Nicolau, Aaron Petronico, Kendra Letchworth-Weaver, Yasaman Ghadar, Richard T. Haasch, Julio A. N. T. Soares, Ryan T. Rooney, Maria K. Y. Chan, Andrew A. Gewirth,* and Ralph G. Nuzzo**

**In this work, the preparation and characterization of modified $LiMn_2O_4$ (LMO) cathodes utilizing chemisorbed alkylphosphonic acids to chemically modify their surfaces are reported. Electrochemical methods to study ionic and molecular mobility through the alkylphosphonate self-assembled monolayers (SAMs) for different alkyl chain compositions, in order to better understand their impact on the lithium-ion electrochemistry, are utilized. Electrochemical trends for different chains correlate to trends observed in contact angle measurements and solvation energies obtained from computational methods, indicating that attributes of the microscopic wettability of these interfaces with the battery electrolyte have an important impact on ionic mobility. The effects of surface modification on Mn dissolution are also reported. The alkylphosphonate layer provides an important mode of chemical stabilization to the LMO, suppressing Mn dissolution by 90% during extended immersion in electrolytes. A more modest reduction in dissolution is found upon galvanostatic cycling, in comparison to pristine LMO cathodes. Taken together, the data suggest that alkylphosphonates provide a versatile means for the surface modification of lithium-ion battery cathode materials allowing the design of specific interfaces through modification of organic chain functionalities.**

## 1. Introduction

Over the past three decades, Li-ion batteries (LIB) have become the most important energy storage technology adopted by the portable electronics and electric vehicle industries due to their high capacity, stability, and high voltage when compared to other batteries.[1]

One feature which allows the lithium-ion battery to achieve stable operation at high voltages is the formation of the so-called solid-electrolyte interphase (SEI). The SEI, whose importance is well established for the anode of LIBs,[2] forms as a result of degradation reactions occurring between the electrode and the electrolyte.[2] At the anode, these reactions result in the formation of a thin, electrically insulating, $Li^+$-conductive material. This electrically insulating layer provides kinetic stability to the battery system.[2] At the cathode, these reactions also yield a protective coating, the nature and function of which depends on specific battery chemistry.[2] For example, it has recently been shown that the cathode interphase can incorporate Mn ions released from a $Li_xNi_{0.5}Mn_{1.5}O_4$ (LMNO) cathode into its structure, in the form of complexes with organic carbonates,[3] thus preventing Mn migration to the anode where it negatively impacts battery performance.[4]

The SEI is composed of two different components: a hard, inorganic layer and a soft, organic layer. The inorganic interphase is believed to be composed of lithium fluoride, lithium oxide, and carbonate salts formed from the decomposition of the inorganic salts ($LiPF_6$, $LiBF_4$, $LiClO_4$, etc.) and organic carbonates (propylene carbonate (PC), ethylene carbonate (EC), dimethyl carbonate (DMC), etc.[2,5,6] The organic part of this layer comprises organic polymers, believed to be a mixture of polycarbonate and polyether molecules.[5] Attempts at controlling growth and composition of the SEI have been made through use of different electrolytes, or by incorporation of additive molecules.[2]

Although the natural SEI affords kinetic stability to the lithium-ion battery system, other degradative pathways are still

B. G. Nicolau, A. Petronico, R. T. Rooney, Prof. A. A. Gewirth, Prof. R. G. Nuzzo
Department of Chemistry
University of Illinois at Urbana-Champaign
Urbana, IL 61801, USA
E-mail: agewirth@illinois.edu; r-nuzzo@illinois.edu

Dr. K. Letchworth-Weaver, Dr. M. K. Y. Chan
Center for Nanoscale Materials
Argonne National Laboratory
Lemont, IL 60439, USA

Dr. Y. Ghadar
Argonne Leadership Computing Facility
Argonne National Laboratory
Lemont, IL 60439, USA

Dr. R. T. Haasch, Dr. J. A. N. T. Soares
Frederick Seitz Materials Research Laboratory
University of Illinois at Urbana-Champaign
Urbana, IL 61801, USA

The ORCID identification number(s) for the author(s) of this article can be found under https://doi.org/10.1002/admi.201701292.

**DOI: 10.1002/admi.201701292**

 

present, particularly at the cathode. For example, in lithium manganese oxide (LMO) cathodes, capacity fade is related to the release of $Mn^{2+}$ into the electrolyte.[7] Several different modifications of the LMO surface have been developed to prevent this dissolution, including surface oxides,[8] thin gold shells,[9] and graphene sheets.[10] In the current work, we examine the use of SAMs comprised of covalently attached alkylphosphonate adsorbates as a means to tune the surface and interfacial chemistry of LMO cathode materials to provide specific functionality.

The modification of metal oxide surfaces with SAMs has been widely investigated with notable exemplars utilizing molecules such as silanes, amines, carboxylic acids, and alkylphosphonic acids.[11] Out of these different classes of molecules, phosphonic acids have been utilized extensively in the past to coat metal oxide surfaces ($TiO_2$ and ITO) used in devices such as sensors and light-emitting devices.[11–14] A previous study utilized a fluoroalkyl silane molecule to modify lithium manganese nickel oxide (LMNO).[15] Here, we use the flexibility attendant of the alkylphosphonate platform to investigate the effect of different functionalities on LMO battery properties.

In this work, we examine different properties of the LMO surface chemistry including wettability, electronic, and lithium-ion conductivity. We tune that behavior by utilizing a series of alkylphosphonates with increasing chain size (butyl phosphonic acid (BPA), decyl phosphonic acid (DPA), and hexadecyl phosphonic acid (HDPA), or by utilizing a series of alkylphosphonates of similar chain lengths but different functional groups: DPA, 3,3,4,4,5,5,6,6,7,7,8,8,9,9,10,10,10-heptadecafluorodecylphosphonic acid (DFPA), and (2-(2-(2-methoxy)-ethoxy)-ethoxy)-alkylphosphonic acid (G3PA). The structures of the alkylphosphonates utilized in this work can be found in Table S1 (Supporting Information).

## 2. Results and Discussion

### 2.1. Surface Modification and Characterization of Model Alkylphosphonate Supported on Lithium Manganese Oxide

#### *2.1.1. Effect of Surface Modification on LMO Cyclic Voltammetry*

In order to characterize the phosphonate-modified LMO interface, we performed cyclic voltammetry (CV) measurements in an electrolyte containing ferrocene (Fc). Fc is a probe reporting on the electrochemical accessibility of the electrode.[16] **Figure 1** shows a series of CVs obtained from thin LMO film cathodes immersed in a solution consisting of 1 M $LiClO_4$ + $3 \times 10^{-3}$ M Fc in PC. CV studies in EC:DMC $LiPF_6$ were also attempted but the films were found not stable in that system. The origin of the instability may be the presence of HF from hydrolysis of the $PF_6^-$ electrolyte which could damage the very thin cathodes.[2] The CVs exhibit two features. The first, in the region marked 1, is associated with the 1 $e^-$ transfer which converts Fc (at ≈3 V) to $Fc^+$ at more positive potentials. For LMO, the peak splitting between the anodic and cathodic waves was ≈140 mV, with larger splitting seen with different coatings. The second, in the region marked 2, is associated with the lithiation and delithiation of the LMO. The figure shows that different surface

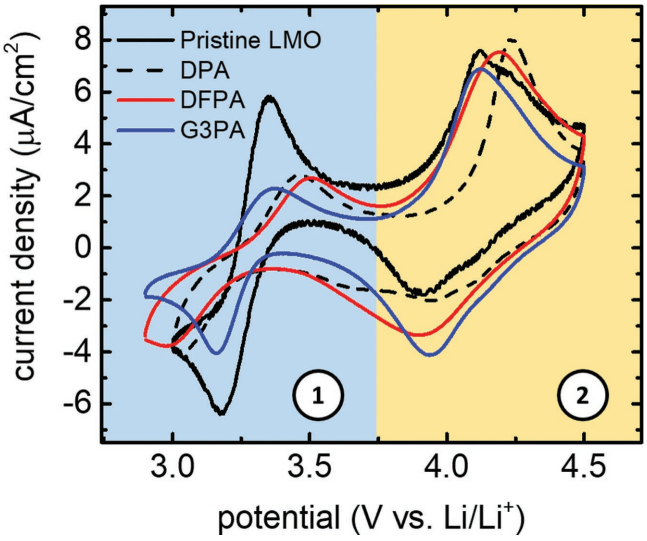


**Figure 1.** Cyclic voltammetry measurements of alkylphosphonate-modified $LiMn_2O_4$ thin films in 1 M $LiClO_4$ in PC electrolyte (with added $3 \times 10^{-3}$ M ferrocene) measured at a scan rate of 0.2 mV $s^{-1}$. Two different redox pairs are observed, containing information about the ferrocene oxidation (region 1) and lithiation/delithiation (region 2).

coatings lead to different behavior in the voltammogram in both regions 1 and 2.

We first address changes in the voltammogram with different surface coatings in region 1. **Figure 2** reports on the changes in anodic peak potentials (Figure 2a) and splitting (Figure 2b) for the Fc probe on the bare and modified LMO surface. Figure 2a shows that the anodic peak potential associated with the $Fc/Fc^+$ couple in this solvent/electrolyte system occurs at 3.27 V versus $Li/Li^+$ for LMO or a control glassy carbon electrode, and 3.28 V on Au controls (Figure S1a, Supporting Information).

The plots in Figure 2 demonstrate that as the alkyl chain length increases, the anodic peak potential becomes more positive and its magnitude increases as well. The magnitude of the splitting seen in the $Fc/Fc^+$ voltammetry correlates with the kinetic barrier of the electron transfer event.[17] Slowing the scan rate 10× leads to electron transport dynamics across the alkylphosphonate layer that more closely resemble that associated with a reversible redox couple (Figure S1b, Supporting Information). We note that, even without an alkylphosphonate layer, the peak splitting is ≈140 mV, which is considerably larger than the 59 mV expected for this one-electron couple. This larger splitting suggests that electron transfer is intrinsically inhibited within the LMO film itself, consistent with the high resistivity (≈5 MΩ) measured in the as-prepared thin film. This high resistivity is due to the insulating properties of LMO, in which conduction occurs via thermally activated polaronic hoping between $Mn^{3+}$ sites.[18,19] In contrast, peak splitting seen for the Fc couple at Au and glassy carbon interfaces is closer to the expected (ideal) values (80 and 65 mV, respectively). The origin of the larger split on Au is ascribed to the strong interactions that occur between the Au electrode and components of the organic electrolytes (which form a blocking layer inhibiting electron transfer).[20]

The electrochemical properties of thin film Au electrodes modified with alkane thiol SAMs have been extensively

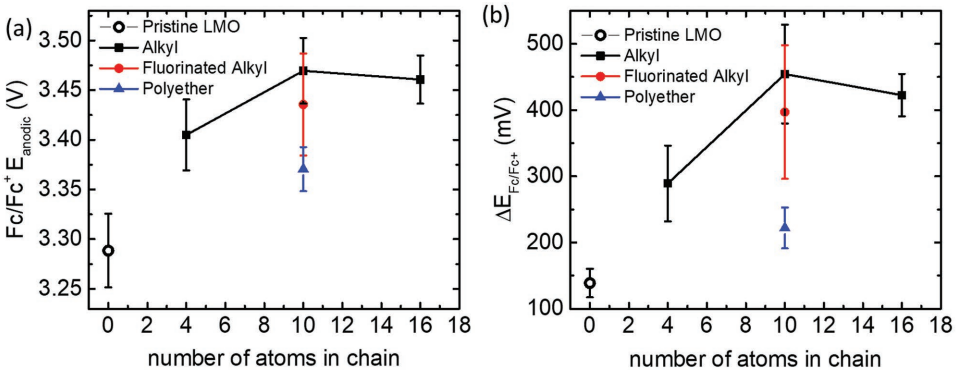


**Figure 2.** Effect of the alkylphosphonate SAMs on the $Fc/Fc^+$ oxidation a) potential and b) peak splitting, obtained from the CVs of coated $LiMn_2O_4$ thin films in 1 M $LiClO_4$ in PC electrolyte, measured at scan rate of 0.2 mV $s^{-1}$, as a function of the ligand's chain length.

studied.[17,21,22] The peak splitting of Fc is known to vary in alkane thiol modified electrodes as a function of alkane chain length ($n$).[17] A perfectly crystalline SAM grown on an atomically flat surface with chain lengths greater than 14 methyl groups leads to full suppression of Fc electrochemistry.[21] This suppression arises because Fc cannot closely approach the Au electrode through a defect-free SAM of that chain length, for which the through-chain electron tunneling rate is low. The Fc redox activity is not suppressed, however, on electrodes consisting of SAMs grown on rougher surfaces due to the presence of defects which allow direct approach of the Fc to the Au surface. In this case, increasing chain length does not result in fully suppressed Fc electrochemistry. Nonetheless, the presence of the SAM does impact the Fc redox activity, which becomes less facile as chain length increases.[17]

The thin film LMO surfaces utilized in this work exhibit a roughness (peak to valley) of ≈50 nm (Figure S2, Supporting Information). Roughness of this magnitude would preclude the formation of densely packed phosphonate monolayers, and would allow Fc oxidation to occur in the presence of a SAM. We note in support of this that there is little change seen in either the peak splitting or the anodic onset potential between alkyl chains with $n = 10$ and 16. The current data do not discriminate whether it is intrinsic defects in the LMO thin film or more complex conformational dynamics in the SAMs that mediate these structure–property correlations.

Also provided in Figure 2 are data for the effect of LMO surface modification by phosphonate SAMs comprised of fluorinated and polyether chains. For similarly sized alkyl chains ($C_{10}$ alkyl, fluoroalkyl, and $C_7O_3$ polyether), the $Fc/Fc^+$ couple exhibits greater reversibility for the polyether relative to the alkyl chain, with the fluorinated chain exhibiting a somewhat intermediate effect. The possible origins of this behavior will be discussed below.

**Figure 3**a shows a plot of the peak splitting measured for the first lithium intercalation redox pair for both the bare and modified LMO surfaces (i.e., region 2 in Figure 1). The peak splitting value obtained for the bare LMO surface is similar to that previously reported for thin films deposited via RF magnetron sputtering.[23] As with the $Fc/Fc^+$ case, an increase in alkylphosphonate chain length results in an increase in peak splitting up until $n = 10$. As with the Fc probe, there is little difference in peak splitting found for SAMs prepared using chain lengths between $n = 10$ and 16, likely for reasons similar to those discussed above.

Further chemical modifications of the chain structure result in behavior comparable to that observed for Fc. The phosphonate SAMs comprised of $C_{10}$ fluorinated chain (DFPA) exhibits a reversibility for lithiation similar to that found with the alkyl chain of the same length. The polyether variant, however, exhibits a lithiation activity similar to that of the pristine LMO surface. This observation suggests that $Li^+$ conductivity

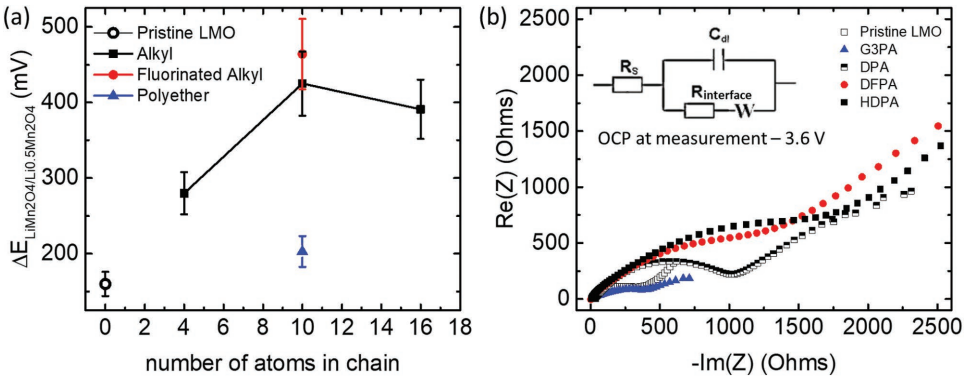


**Figure 3.** a) Effect of alkylphosphonate SAMs on the lithium intercalation reaction peak splitting, obtained from the CVs of coated $LiMn_2O_4$ thin films in 1 M $LiClO_4$ in PC electrolyte, measured at scan rate of 0.2 mV $s^{-1}$. b) Impedance measurement results for different coated interfaces and the Randles circuit (inset).

in the polyether SAM is much more facile relative to the alkyl and fluorinated analogs. We note with interest that the main constituent of the organic speciation of the cathode solid-electrolyte interphase is in fact poly(ethylene glycol) dimethyl ether formed via an electrochemically mediated oligomerization process involving the EC solvent. Such moieties are similar in composition to the long polyether chain.[5]

#### 2.1.2. Impedance Measurements

The interfaces of the modified LMO films were further characterized with electrochemical impedance spectroscopy. Figure 3b shows Nyquist plots of the measured impedance for different modified interfaces, obtained at open circuit potential (OCP), prior to cycling. The impedance spectrum obtained for the pristine LMO surface is in agreement with values observed for LMO cathodes in the past.[24] Figure 3 shows that in most cases, surface modifications by the SAMs result in an increase in the measured impedance. The exception to this trend is the surface modified with a G3PA SAM, which shows behavior very similar to the uncoated LMO. The impedance spectra were fit to a simplified Randles circuit (see Figure 3b inset) and resistivity values were obtained for each modified interface. The resistivity of lithium battery cathodes in the frequency range utilized (1 MHz to 10 Hz) is typically attributed to conductivity of both electronic and ionic ($Li^+$) components through the interface as well as through the solid-electrolyte interphase.[25,26] The simplified Randles circuit is usually augmented by more sophisticated models;[25] the fits made here are utilized to obtain trends. In the case of an uncycled cell with an OCP ≈ 2.6 V lower than the potential of oxidation of the PC solvent,[27] the resistivity values are associated mainly with electronic and ionic conduction at the interface. The values obtained for $R_{interface}$ (where $R_{interface}$ is the total resistivity of the interface, including the charge transfer resistance ($R_{CT}$), the resistance of the cathode-electrolyte interphase ($R_{CEI}$), and the alkylphosphonate SAM resistance ($R_{SAM}$)) for pristine LMO, DPA, DFPA, G3PA, and HDPA were 230, 550, 870, 270, and 960 Ω, respectively. As expected, the $R_{interface}$ increases with an increase in the length of the alkyl chain.[28] The difference in $R_{interface}$ seen between the similar chain length compositional series exhibits a trend similar to the results observed for the lithium intercalation dynamics (Figure 3a): the polyether chain presents the least resistivity, the alkyl chain an intermediate value, and in this case, the fluoroalkyl chain presents the highest resistivity.

#### 2.1.3. X-Ray Photoelectron Spectroscopy (XPS) Measurements

The data presented above show that the electrochemical properties of the SAM-modified LMO substrates exhibit a dependence on both the chain length and composition of the modifying phosphonate adsorbate. The quantitative behaviors seen there likely arise from changes in the structure/adsorbate coverage as a result of different phosphonate adsorbates. Such differences likely lead to the different interface permeabilities noted for the Fc and $Li^+$ electrochemical probes studied above.

We carried out XPS studies to independently establish and correlate the association of modifications of the electrochemistry of the LMO surfaces with the surface coverage of the alkylphosphonates present in the SAM. Exemplary XPS data are shown in **Figure 4**a–c that allow an analysis on this basis. To facilitate comparison, the *y*-axes of these spectra have been offset and normalized to reflect the relative atomic concentration of the three elements (see the Supporting Information). Figure 4a shows the Mn 2p region characteristic of $LiMn_2O_4$[29] and is consistent with Mn present as a mixture of $Mn^{3+}$ and $Mn^{4+}$.[30,31] The C 1s spectra, shown in Figure 4b, indicates the presence of core level peaks expected for the distinct molecular structure of each alkylphosphonate adsorbate: C—C (285.0 eV), C—O (286.6 eV), $CF_2$ (291.4 eV), and $CF_3$ (293.7 eV).[32] The suggested assignments of O—C=O (288.9 eV) and C—O peaks in the HDPA spectrum suggest the presence of a minor surface impurity within that SAM (likely in part due to an adventitious uptake of $CO_2$ as a carbonate moiety). The P 2p spectra shown in Figure 4c establish that the phosphorous present is in fact bound as a phosphonate (132.8–133.2 eV).[32,33]

In order to evaluate the surface coverages of the various adsorbates, the thicknesses of the monolayers were estimated using a procedure similar to that described previously in the literature.[34–37] This two-layer model simplifies the properties associated with a thin attenuating overlayer (the SAM chain, which is assumed to be thin compared to the mean free path at the relevant photoelectron energies) to evaluate the intensities of the P 2p and Mn 2p signals, in order to extract the molecular density of a phosphorus containing SAM adsorbate standing on top of a quasi-infinite layer of manganese bound within the LMO substrate. This approximation is sufficient to provide a good qualitative measure of adsorbate related structure/property trends seen between the different SAM coatings.

Coverage estimates determined using the two-layer model are shown in Figure 4d and summarized in **Table 1**. Within the range of the errors, the adsorbate coverages estimated for all coatings are within the same order of magnitude, falling within the mid-range of $10^{13}$ molecules $cm^{-2}$. We note that the value obtained from modeling shows that the coverage differences between coatings are all similar within a factor of 3. Such small differences in coverage are likely not sufficient to explain the trends observed in both experiments and calculations. By way of comparison, alkylphosphonate coverages reported in other studies range from coverages of $10^{11}$–$10^{13}$ molecules $cm^{-2}$.[35–37] From these data we conclude that the differences seen in the electrochemical properties of the variously SAM-modified LMO electrodes cannot be simply ascribed to differences in the coverage of the alkylphosphonate adsorbates. This suggests that, while the SAMs do function as a barrier layer, other features/dynamical effects may also play a role in mediating the structure/rate and structure/property correlations seen.

#### 2.1.4. Contact Angle Measurements

We made contact angle measurements to provide information about how the various SAMs impact the interaction of the LMO substrate with representative LIB electrolytes.[38] The data in **Figure 5** represent the contact angles measured for each of

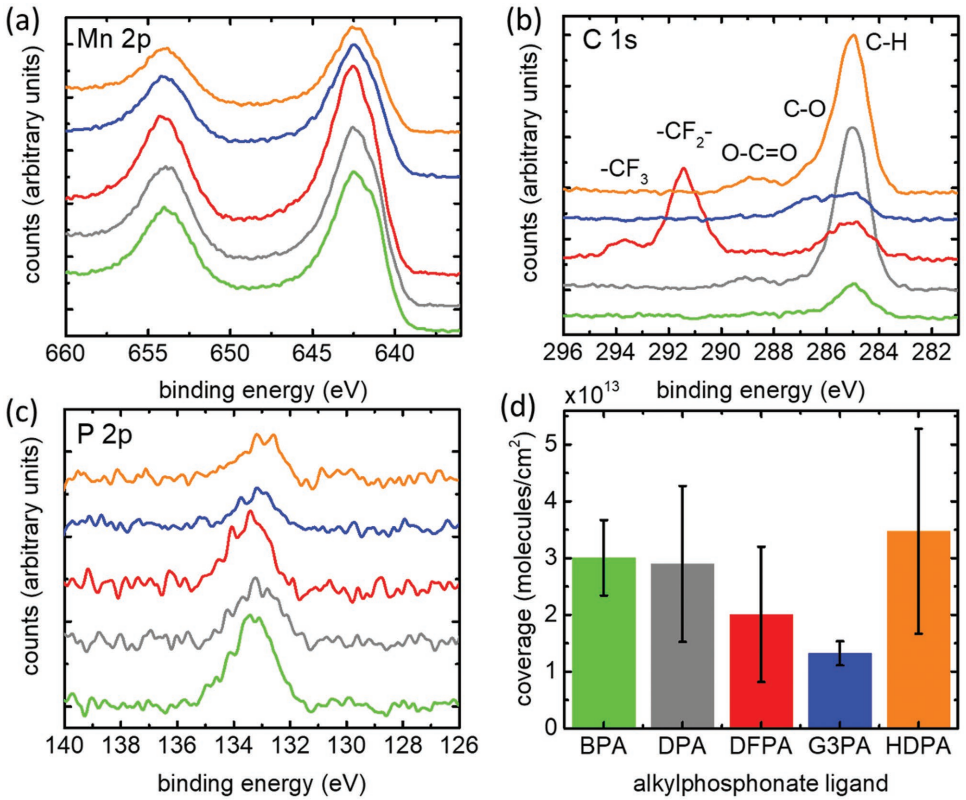


**Figure 4.** XPS of a) Mn 2p, b) C 1s, and c) P 2p data from the principal elements of the alkylphosphonate monolayer surfaces stacked vertically in the following order: BPA-green (bottom), DPA-gray, DFPA-red, G3PA-blue, and HDPA-orange (top). d) Alkylphosphonate monolayer surface coverage as determined using the two-layer model.

the SAMs in two different electrolyte systems: 1 M $LiClO_4$ in PC solvent and 1 M $LiPF_6$ in EC:DMC (1:1) solvent. The images in Figure 5a show representative profiles of electrolyte sessile droplets standing on the same films utilized for the XPS measurements.

Figure 5b shows a plot of the contact angle ($\theta_s$) values obtained with a PC/$LiClO_4$ electrolyte on the SAM-modified LMO cathodes. The observed $\theta_s$ values range from 27° (G3PA, indicating wetting affinity for the surface) to 90° (DFPA, indicating nonwetting condition). The data in Figure 5b indicate that the contact angle increases as the length of the alkyl chain increases up to $n = 10$, which exhibits nearly the same contact angle as the $n = 16$ SAM. The similarities between the latter two in wetting behaviors mirror those in their CV data in this electrolyte.

Figure 5c shows the values of $\theta_s$ measured for the EC:DMC electrolyte system. The contact angles measured in this case range from 30° (G3PA, highest wettability) to 75° (DFPA, lowest wettability). Again, $\theta_s$ (Figure 5c) increases with chain length, albeit to a smaller degree than with PC/$LiClO_4$. It is important to note, however, that in EC:DMC, an increase in the alkyl chain from $n = 10$ to 16 results in an increase in contact angle and consequently a decrease in electrolyte affinity with the surface.

The contact angles measured show a good correlation with the trends observed in Figures 2 and 3, which suggests that electrolyte affinity with the modified LMO substrate is an important factor defining the permeability of electroactive species through the barrier-layer SAMs, as proposed above. Attentive structure–property/structure–rate correlation would

**Table 1.** XPS peak area, relative atomic concentration, and deduced coverage.

| Alkylphosphate | Peak area [count eV $s^{-1}$] | | | Atomic concentration [%] | | | Coverage [$10^{13}$ molecules $cm^{-2}$] |
|---|---|---|---|---|---|---|---|
| | $I_{Mn}$ | $I_C$ | $I_P$ | $N_{Mn}$ | $N_C$ | $N_P$ | |
| BPA | 16 148.2 | 604.8 | 273.1 | 68.9 ± 5.7 | 24.7 ± 6.1 | 6.4 ± 1.9 | 3.0 ± 0.6 |
| DPA | 15 910.4 | 2612.8 | 259.5 | 37.6 ± 1.1 | 59.1 ± 1.4 | 3.4 ± 1.7 | 2.9 ± 1.4 |
| DFPA | 20 160.5 | 2341.8 | 227.6 | 46.0 ± 2.8 | 51.1 ± 2.9 | 2.8 ± 1.9 | 2.0 ± 1.2 |
| G3PA | 12 728.6 | 700.2 | 94.6 | 63.8 ± 5.2 | 33.6 ± 5.4 | 2.6 ± 0.6 | 1.3 ± 0.2 |
| HDPA | 8973.0 | 2770.9 | 175.3 | 24.6 ± 0.6 | 72.7 ± 1.2 | 2.6 ± 1.4 | 3.5 ± 1.8 |

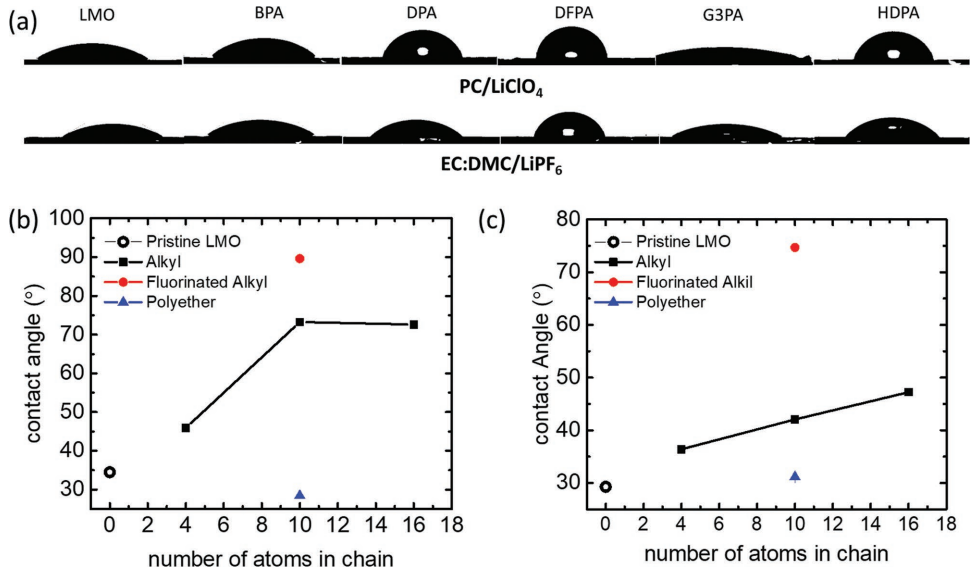


**Figure 5.** Contact angle measurements on coated LMO thin films in two different electrolyte systems: 1 M $LiClO_4$ in propylene carbonate and 1 M $LiPF_6$ in ethylene carbonate/dimethyl carbonate 1:1 solvent. a) Recorded image of solvent droplets resting on SAM-modified LMO surfaces; fitted contact angle parameter by the Rame-Hart software for b) $LiClO_4$/PC and c) $LiPF_6$/EC:DMC.

associate poorer wettability with less effective transport of electroactive species present in the electrolyte, including $Li^+$ ions.

### *2.1.5. Computational Studies of Alkylphosphonate-Modified LMO*

We used atomistic and first principles modeling to provide further, more quantitative insight into the formation, stability and wettability of LMO surfaces coated with alkylphosphonate SAMs. Because the solubility of the phosphonates in the electrolyte determines the relative stability of the SAM on the oxide surface upon electrochemical cycling, we computed their solvation free energies in PC with 1 M $LiClO_4$ for comparison. Classical molecular dynamics (MD) simulations were employed to sample the possible conformations of the chains. Snapshots of the alkylphosphonate geometry from the classical MD trajectory were then computed within density function theory (DFT) incorporating a continuum solvation model to represent the instantaneous configuration of the PC electrolyte (see the Supporting Information for additional details on the methodology and computational procedures).

**Figure 6**a and **Table 2** show the calculated solvation energies for different alkylphosphonates as a function of chain composition. The solvation energy of the phosphonic acid form of the adsorbate is computed for reference. Figure 6a shows that an increase in chain length from $n = 4$ to 10 (BPA to DPA) results in a decrease in stabilization of the respective alkylphosphonic acid solute due to an increasing cost of forming a cavity in the liquid of the size of the solute. From $n = 10$ to 16 (DPA to HDPA), the solvation energy remains roughly constant since the additional conformations available to the longer chain cause a decrease in energy which counteracts the increased energetic cost of cavity formation.[39] With respect to alkylphosphonic acids of the same length, Figure 6a shows that the fluoroalkylphosphonic acid (DFPA) has a similar electrolyte affinity to the regular alkyl chain. Alternatively, the polyether-based phosphonic acid (G3PA) shows the lowest solvation energy of all alkyl phosphonic acids simulated, and therefore the highest electrolyte affinity. These solvation energy results are in good agreement with the trends observed in the contact angle measurements and electrochemistry reported above. These results further support the important role electrolyte affinity plays in the modulation of electrochemical properties of LMO cathodes with the addition of alkylphosphonic acid based SAMs.

Figure 6b shows two stable binding conformations of phosphonic acid on energetically favorable (001) LMO surfaces.[40] Two different cases are shown: lithium-poor surfaces and lithium-rich surfaces. In the case of lithium-poor surfaces, two covalent bonds are formed between manganese atoms and the oxygens belonging to the phosphonate (–1.9 eV), with a third, weak O—H—O bond slightly stabilizing the configuration. In the case of a lithium-rich surface, a slightly less stable configuration (–1.6 eV) can also form, consisting of a covalent bond between a lithium atom and the oxygen atom belonging to the phosphonic acid and a strong O—H—O bond. Independent of surface lithium concentration, Figure 6b shows that phosphonic acid will attach to the LMO surface through a bidentate or tridentate bond consisting of one or two covalent metal—O bonds and an O—H—O bond. When a second covalent metal—O bond forms, one of the hydrogen atoms is found to dissociate from the phosphonic acid and adsorb on an LMO surface oxygen atom. The binding energies of the phosphonic acid on the surfaces are computed from the expression

$$E_{\text{bind}} = E_{\text{LMO+PA}} + nE_{\text{LMO+H}} - E_{\text{PA}} - (n+1)E_{\text{LMO}} \quad (1)$$

where $n$ is the number of H atoms which dissociate from the phosphonic acid. The energies $E_{\text{LMO}}$, $E_{\text{LMO+H}}$, and $E_{\text{LMO+PA}}$ are computed for the LMO surface with no adsorbates, adsorbed H,

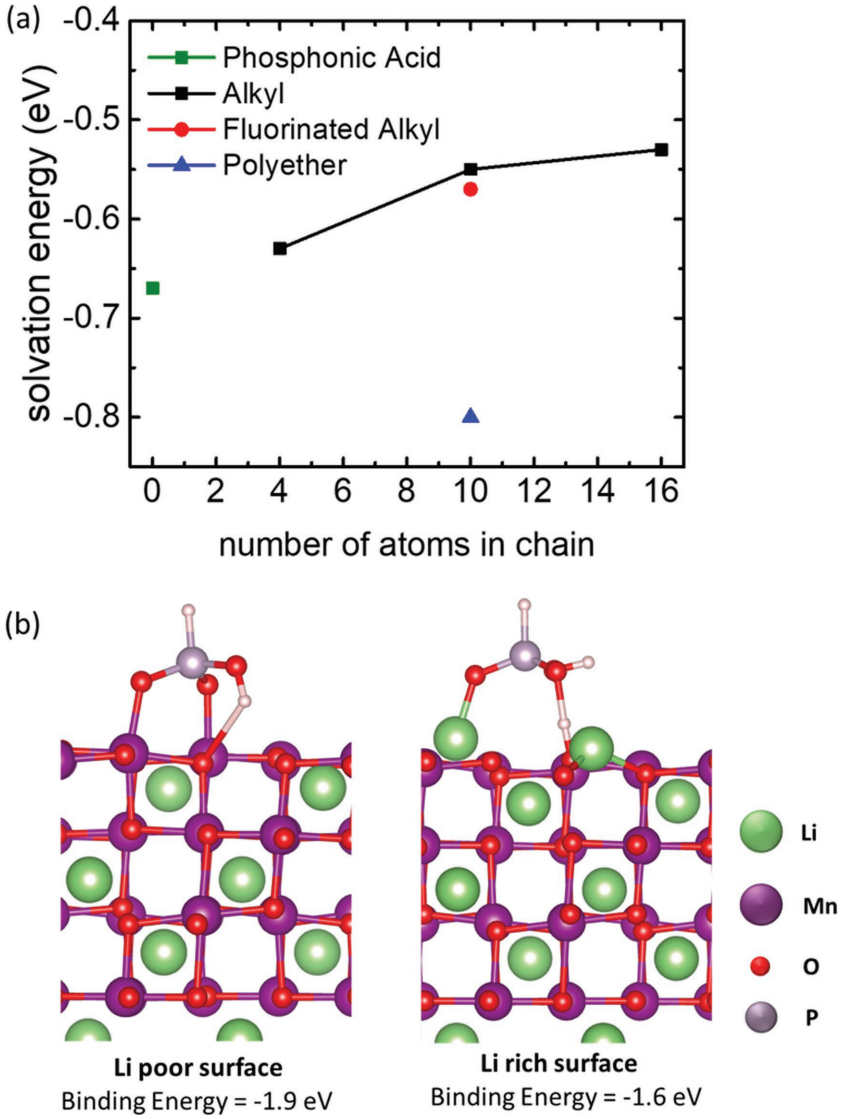


**Figure 6.** a) Calculated solvation energy of different alkylphosphonate species in PC/$LiClO_4$ electrolyte, as determined by DFT. The line is provided as a guide for the eye. b) Binding modes and energies of phosphonic acid on (001) lithium manganese oxide surfaces as determined by DFT calculations. Two different surface conditions, lithium rich (right) and lithium poor (left) are simulated.

**Table 2.** Solvation energies calculated via a combined classical MD and DFT approach for different phosphonic acids in PC/$LiClO_4$ and EC:DMC/$LiPF_6$ (also shown in Figure 6b).

| Alkyl phosphonic acid | Solvation energy in PC/$LiClO_4$ [eV] | Solvation energy in EC:DMC/$LiPF_6$ [eV] |
|---|---|---|
| $H_2PO_3$ | −0.67 | −0.73 |
| BPA | −0.63 | −0.66 |
| DPA | −0.55 | −0.62 |
| HDPA | −0.53 | −0.59 |
| DFPA | −0.57 | −0.56 |
| G3PA | −0.80 | −0.93 |

and adsorbed phosphonic acid, respectively. The energy $E_{PA}$ represents the energy of phosphonic acid in its reference state, either in vacuum or in solution. This expression for binding energy is similar to the one presented in the literature,[41] except hydrogen on the LMO surface was chosen as a reference state rather than $H_2$ gas, due to presence of the electrochemical environment.

**Table 3** reports the binding energies of phosphonic acid in vacuum and in solution, as well as the bond lengths for the configurations shown in Figure 6b. The solvation energies for the alkylphosphonates in $LiClO_4$/PC range from −0.5 to −0.8 eV (Table 2), indicating that phosphonic acid in electrolyte is less stable than phosphonic acid bound to the LMO surface. These results indicate that SAMs formed from bonding of phosphonic acids to LMO are stable in lithium-ion battery electrolytes, and that the stability is robust (i.e., able to fully saturate the adsorption isotherm) regardless of the amount of lithium on the surface. Similar results were also observed when calculating the solvation energies of alkylphosphonates in EC:DMC (1:1)/$LiPF_6$, where the energies ranged from −0.7 to 0.8 eV (Table 2), indicating that these SAMs are stable regardless of the electrolyte of choice.

The above alkylphosphonate binding conformations and energies are in reasonable agreement with previous results for alkylphosphonate association with indium tin oxide (ITO) and other materials.[11,41,42] Alkylphosphonate association with ITO is found to occur though oxygen–indium bonds of length 2.2–2.3 Å, with additional O—H—O bonds of length 1.37–1.6 Å. These M—O bond lengths are somewhat larger than those reported in Table 3. Binding energies of phosphonates on ITO range −1.6 to −1.7 eV, independent of coverage and particular binding configurations.[41]

Both the shorter metal–oxygen bonds and the more stable binding energy for phosphonic acid on the LMO surface relative to ITO indicate that the ligands are more strongly bound on LMO. Though it has been found that as coverage increases, the most likely binding configuration may change from bidentate to tridentate, the binding energies on ITO are remarkably constant.[41] This limited role of intermolecular interactions in stabilizing the adsorbate provides support for the approximation to consider only one phosphonic acid per surface LMO unit cell (this coverage is also still within reasonable agreement with the XPS estimated values above).

When taken together, the calculations suggest that: (1) the stability of the monolayer in the electrolyte increases as a function of chain length and (2) stable binding configurations for phosphonate on LMO do exist, similar in type to those found

**Table 3.** Phosphonic acid geometries and binding energies for Li-rich and Li-poor LMO (001) surfaces. Reference states for phosphonic acid in vacuum and solvated in PC/$LiClO_4$ are both considered.

| Surface | Binding energy in vacuum [eV] | Binding energy in PC/$LiClO_4$ [eV] | Binding mode | Bond length [Å] | Bond angle [°] |
|---|---|---|---|---|---|
| Li-rich LMO (001) | –1.6 | –1.0 | 1 Li—O | 1.85 | – |
| | | | 1 O—H—O | 2.53 | 176° |
| Li-poor LMO (001) | –1.9 | –1.2 | 2 Mn—O | 1.95, 1.96 | – |
| | | | 1 O—H—O | 2.84 | 120° |

previously for ITO; (3) the binding energies are sufficient to lead to high adsorbate coverage in the SAM.

### 2.2. Effect of Surface Modification on Battery Behavior

We next evaluate the effects of LMO surface modification with the alkylphosphonic acids on battery performance. Such coatings may be adventitious for a number of reasons. The coating may stabilize or alter the SEI. It may also stabilize the electrode material. Lithium-ion batteries utilizing LMO as a cathode are known to fade in capacity upon galvanostatic cycling.[9,10] This capacity fade is attributed to both chemical corrosion by HF species formed from hydrolysis of $LiPF_6$ and the release of $Mn^{2+}$ species into the electrolyte as the crystal lattice of LMO expands upon discharge. The $Mn^{2+}$ species in the electrolyte interact with the SEI on the anode and/or plate on the anode itself, causing performance degradation.[7]

We emphasize that the modified cathodes studied in this section have fundamental differences from the model systems analyzed in Section 2.1. In this section, we examine composite slurries to which carbon and a binder were added to the cathode materials. In Section 2.1, we used binder- and carbon-free thin films of LMO. The additional interactions present in the composite will likely change the overall behavior of the cathode system. As a control we have independently characterized phosphonate coverage on coated particles through XPS. Results indicate the same degree of coverage in both systems, as shown in Table S5 (Supporting Information).

#### *2.2.1. ICP-MS Studies of Mn Dissolution*

**Table 4** shows the concentration of Mn in recovered electrolyte following 72 h immersion of modified LMO particles (≈250 mg) in of 1 M $LiPF_6$ electrolyte in EC:DMC (1:1) solvent (11 mL) at room temperature.[9] The recovered electrolyte was obtained by centrifugation at 3300 rpm and filtration of the supernatant electrolyte through a 0.3 μm PTFE filter.

**Table 4.** Room temperature Mn dissolution study via ICP-MS.

| Alkyl phosphonic acid | Amount of Mn detected [ng $L^{-1}$] | % less Mn dissolved relative to pristine LMO [%] |
|---|---|---|
| Pristine LMO | 146 | – |
| BPA | 117 | 20 |
| DPA | 100 | 32 |
| HDPA | 13 | 91 |
| DFPA | 104 | 29 |
| G3PA | 163 | –11 |

Table 4 shows that the Mn concentration in the recovered electrolyte decreases drastically with an increase in the chain length of the decorating alkylphosphonate. We suggest that the longer chain length leads to less exposure of the LMO surface to the solvent, essentially terminating it as an insoluble metal oxide phosphonate complex and thus diminishing the amount of $Mn^{2+}$ that can be dissolved. Interestingly, the contact angle measurements showed a similar trend, with longer alkylphosphonates yielding higher contact angles. All the alkylphosphonate-modified particles dissolve less Mn relative to the bare material, with the exception of the G3PA. Apparently, G3PA enhances Mn dissolution, albeit only slightly. This effect may be due to the increased solvent accessibility through this material, discussed above. Interestingly, DFPA blocks Mn dissolution to the same extent as the same chain length DPA, while contact angle measurements suggest that DFPA decoration leads to minimal solvent exposure. As we posit that $Mn^{2+}$ dissolution in the SAM-modified LMO is a defect-driven process, in that single sites are the locus of Mn dissolution activity, the contact angle measurements reflect more on the overall passivation of the substrate toward its interactions with the electrolyte solvent. This result suggests that the defect density in the DFPA SAMs is likely to be similar to those present in the DPA system.

#### *2.2.2. Galvanostatic Cycling*

We also compare the behavior of surface-modified LMO in a lithium-ion half-cell during galvanostatic cycling. This allows us to observe the impact of surface modification on battery operation, as well as test the Mn retention observed in the previous section by observing the change in capacity following 100 battery cycles. **Figure 7**a shows capacity retention curves obtained from galvanostatic cycling experiments for half-cells utilizing composite cathodes containing the modified LMO particles. Figure 7a shows that the maximum capacity obtained from these modified cathodes is altered by the presence of any alkylphosphonate coating. Uncoated LMO exhibits the highest overall capacity, while BPA-, DFPA-, DPA-, and G3PA-modified LMO exhibit lower capacities. The lowest overall capacity was obtained for the 16-member alkylphosphonate (HDPA). Clearly, the HDPA is most effective at blocking $Li^+$ access to LMO. The other phosphonates all block $Li^+$ access to some degree.

Figure 7 also shows the impact of cycling rate on the capacity of cathodes modified with alkylphosphonates of similar chain length. The magnitude of the capacity loss with increasing

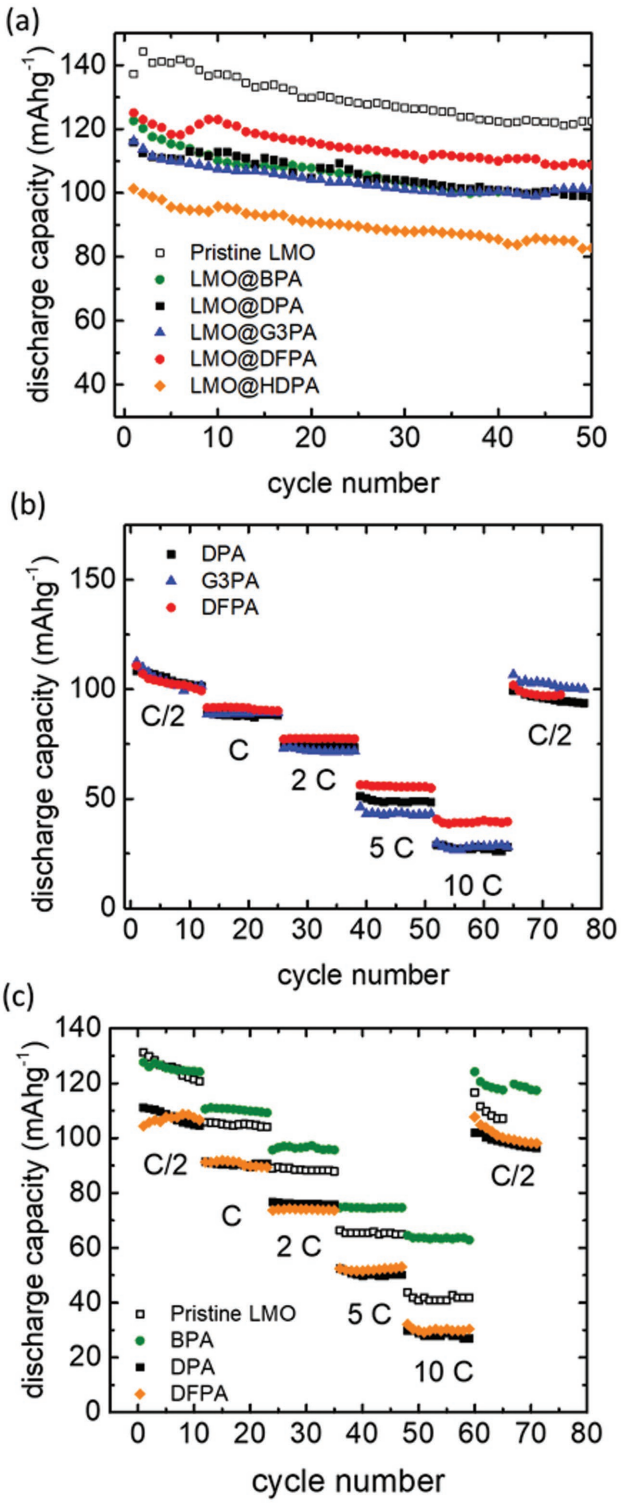


**Figure 7.** a) Cycling experiments on lithium-ion half cells. Cathodes comprised of pristine LMO, and phosphonic acid (DPA, DFPA, HDPA, and G3PA) coated particles. All cells were cycled in 1 M $LiPF_6$ in EC:DMC electrolyte at a rate of 0.5 C. b) Cycling behavior of three different SAMs with the same chain length (DPA, G3PA, and DFPA) as a function of cycling rate. c) Cycling behavior of three different SAMs of different chain length (BPA, DPA, and HDPA), as well as behavior of uncoated LMO as a function of cycling rate.

cycling rate is related, in part, to the permeability of the different artificial interfaces. Figure 7b shows that in the case of galvanostatic cycling, permeability is (most strikingly) higher for fluoroalkylphosphonates and lower for polyether modifications. Figure 7c shows the galvanostatic discharge capacity as a function of rate for surfaces coated with alkylphosphonates of different chain length. HDPA and DPA-coated surfaces show similar rate performance compared to the pristine surface. The particles coated with BPA showed the highest improvement in capacity at a rate of 10 C.

The galvanostatic cycling data indicate that although surface modification will lead to an overall loss of capacity, one somewhat correlated to the alkylphosphonate chain length, it can also lead to improvements in other aspects of battery performance, such as allowing fast charging and discharging of a battery.

Table S6 (Supporting Information) shows the effect of surface modification on the capacity retention upon battery cycling. After 50 cycles (at a rate of 0.5 C), capacity loss can be observed for all the different systems studied. We show that there are differences between the capacity retention of pristine LMO and alkylphosphonate covered LMO. Capacity fade upon cycling was observed independent of which coating was utilized. The pristine LMO particles show the largest capacity fade after 100 cycles, with a capacity retention of 82%. The coated LMO particles show slightly improved capacity retention. The capacity fade observed for all coated particles is reduced by ≈5% compared to uncoated LMO, independent of the ligand type. The behavior of the G3PA coating during cycling is different from that reported in the previous section, where increases in Mn dissolution were seen compared to pristine particles. The different behavior can be explained by the differences between experiments. Immersion studies in the previous section utilize free particles in large amount of solvents, while the galvanostatic cycling reported in this section utilizes a complex slurry electrode (LMO, PTFE binder, carbon) and very small quantities of electrolyte.

Comparing these results to those observed in Table 4, it is apparent that although the coatings provide substantial protection from chemical etching, with a reduction in Mn dissolution of up to ≈90%, their effects on capacity retention upon long-term cycling are rather more modest.

## 3. Conclusion

This work shows that the interfacial properties of LMO cathodes are tunable by the decoration of the metal oxide surface with different alkylphosphonates. We showed that the wettability of the alkyl chain by the solvent plays a key role in facilitating the transport of molecules and ions through the phosphonate layer. We also showed that the difference in surface coverage between different alkyphosphonate coatings, modeled from XPS data, is likely too small to account for the trends observed. Interfaces crafted from polyether-based alkylphosphonates allow $Li^+$ ion transport similar to that seen with unmodified thin film LMO. The transport of ions is influenced by the chain length of the alkylphosphonate and the presence of defects in the film.

DFT calculations show that phosphonic acid association with the LMO surface mimics that found when these molecules decorate other oxides such as ITO. A bidentate Mn—O bond, further stabilized by an O—H—O bond, seems to be the most likely configuration out of those studied in this work. When compared to the solvation energies of the precursor alkylphosphonic acids, the binding energies obtained suggest that the phosphonic acid modified LMO should be stable when immersed in the battery electrolyte, consistent with experiment.

Battery cycling studies show that the presence of hydrophobic chains at the surface of LMO leads to decreased Mn dissolution. During galvanostatic cycling, we found improved rate performance for one coating (15–60% higher capacity at 5–10 C), and up to 5% improvement in capacity retention at 100 cycles for all coatings, compared to the pristine particles. It is important to note that the viability of this new form of LMO coating for the control of interfaces requires more studies. As one example, the behavior of these coatings and their performance at higher temperatures is still required and will be the subject of future work.

In conclusion, we demonstrated that modifying LMO cathodes enable interfacial property tuning through changes in the functional groups present in the precursor molecules. We suggest that, with careful design choices, it may be possible to create SAMs that further improve rate performance or capacity retention.

## 4. Experimental Section

*Decoration of $LiMn_2O_4$ Films and Particles with Alkylphosphonate SAMs*: Thin film LMO cathodes were prepared via RF magnetron sputtering using a modification of a previously reported methods.[23,43,44] A stoichiometric lithium manganese oxide plate (LTS Research Laboratories, Inc.) was used as the target. Pure argon was utilized to generate a plasma at a chamber pressure of 5 mTorr. The RF power applied to the target was 75 W. Polished 0.5 in. diameter stainless steel discs were used as substrates for samples utilized in electrochemical experiments. The stainless steel acts as a current collector and provides a smooth, albeit disordered, surface for deposition. RF sputtering deposition of LMO on the stainless-steel substrate took place for a period of 16 h. The amorphous films obtained were then annealed at a temperature of 700 °C for 1.5 h. The resulting polycrystalline films were evaluated by profilometry and scanning electron microscopy. Films exhibited thicknesses of ≈300 nm and surface roughness on the order of 30 nm.

Thin films of LMO and LMO particles (Sigma-Aldrich, electrochemical grade) were coated with alkylphosphonate SAMs. Alkylphosphonic-modified surfaces were prepared by immersion of LMO (films and particles) in $10 \times 10^{-3}$ M ethanol solutions of phosphonic acids for a period of 12 h. The samples were then recovered and washed with copious amounts of ethanol in order to remove any physisorbed molecules from the surfaces. The resulting modified LMO was then dried under vacuum at 70 °C. Phosphonic acids used were BPA (Sigma-Aldrich, 98%), DPA (Sigma-Aldrich, 97%), HDPA (Sigma-Aldrich, 98%), DFPA (Sigma-Aldrich, > 95%), and G3PA (Sikemia, >97%).

*Electrochemical Characterization*: CV experiments were conducted utilizing a CH Instruments electrochemical workstation (Model 1020C, Austin, TX). The three-electrode cell configuration utilized the thin film LMO cathodes as working electrode and lithium foil (Alfa-Aesar) as the counter/reference. A 1 M lithium perchlorate solution in propylene carbonate was chosen as the electrolyte to minimize the formation of natural solid-electrolyte interphase.[2,27,45] CV experiments were carried out in an argon atmosphere glovebox, where both oxygen and water concentrations were ≈1 ppm.

Potentiometric electrochemical impedance spectroscopy (PEIS) experiments were carried out utilizing a BioLogic electrochemical station (model SP-150). These experiments utilized an airtight Swagelok cell configuration, prepared in the glovebox, where the thin film LMO discs were utilized as working electrodes and lithium foil discs as counter/reference electrodes.[46] 1 M $LiClO_4$ in PC electrolyte was utilized in these experiments. The sealed Swagelok cells were removed from the glovebox prior to PEIS experiments and the integrity of the cell was evaluated by CV.

Galvanostatic experiments were run in CR2032 coin cells obtained from MTI Corp. (Richmond, CA). The cell was assembled by first placing a 0.5 in. diameter circular piece of lithium in the base of the cell. A Whatman glass fiber paper (GF/F) was then placed on the lithium as separator and soaked in electrolyte (1 M $LiPF_6$ in 1:1 EC/DMC). The cathode was prepared by grinding the modified LMO particles with 10 wt% PTFE and 20 wt% Ketjen Black carbon in a mortar and pestle and the resulting material was pressed onto an Al mesh current collector. Typical loading was ≈1 mg $cm^{-2}$. The cathode was then placed on top of the separator and a stainless-steel disc was placed on top as a spacer before placing a spring (MTI stainless steel wave spring for the CR2032 case) and the top cap. The cell was then sealed closed using an MTI hydraulic crimper. An MTI cycler (Richmond, CA) was used to cycle the cells. C-rates were calculated using the mass active material in the cathode composite, assuming a working capacity of 130 mAh $g^{-1}$. Capacities are reported as a function of active material in the cathode.

*Characterization of Modified LMO Surfaces*: XPS measurements were made using a Kratos Axis Ultra X-ray photoelectron spectrometer (Kratos Analytical, Inc., Manchester, UK) using monochromatic Al K$\alpha$ radiation (1486.6 eV) at 210 W (15 mA, 14 kV). The samples were affixed onto the sample holder using double-sided copper tape. High-resolution spectra were collected at an emission angle of 0° and a pass energy of 40 eV. The binding energy scale was referenced to the aliphatic C 1s signal at 285.0 eV. Quantitation was done using CasaXPS version 2.3.15 by determining the area under the curve after applying a Shirley background. Sensitivity factors were supplied by the instrument manufacturer. Further details regarding the quantification method can be found in the Supporting Information.

*Computational Details*: Classical MD simulations using the LAMMPS software[47] were used to sample the possible configurations of phosphonate molecules in the electrolyte solution. The construction of the simulation boxes, the nonreactive pair potentials used to represent the short-range interatomic forces, and the procedure for computing long-range electrostatic interactions are described in the Supporting Information. The systems were brought to mechanical and thermal equilibrium at 330 K using the *NVT* ensemble of Nóse and Hoover.[48–50] The systems were simulated using the Verlet algorithm[51] and a 0.5 fs time step for a series of runs of time 0.5 ns until the system temperature and pressure could be verified, then the production run consisted of two consecutive simulations of time 1 ns to obtain reliable statistics.

To compute solvation free energies of the phosphonates, 64 snapshots were randomly chosen from the 1 ns classical MD trajectory for each solute in the PC and EC:DMC electrolytes. The energy of each solute conformation was then evaluated using plane-wave DFT calculations in vacuum and with a continuum description of the surrounding electrolyte, using the JDFTx software and methodology described in the Supporting Information. DFT calculations in the presence of liquid electrolyte were performed within the framework of joint density-functional theory,[52] using an implicit solvent approximation to the full theory known as nonlinear PCM (with parameterizations described in Section S1.3, Supporting Information). This polarizable continuum-like solvation approach replaces the fluid by a local dielectric response and can account for dielectric saturation of the solvent due to high electric field.[53] The solvation energy for each molecule was then computed by determining the difference in total energy between the molecule in liquid and the molecule in vacuum taking an average over the 64 snapshots.

DFT optimization of phosphonate binding to the LMO surface was conducted by placing a phosphonic acid on the low surface energy terminations.[40] A Hubbard $U$ self-interaction correction[54] to the PBE exchange correlation functional[30] was employed for the manganese $d$ orbitals with $U$ = 3.5 eV. A slab supercell of LMO within periodic boundary conditions (as described in the Supporting Information) was constructed. The phosphonic acid was placed on one side of the slab and the atoms on the other side of the slab were fixed to their bulk-like positions. The positions of the free atoms were optimized until total force was less than 10 meV $Å^{-1}$.

## Supporting Information

Supporting Information is available from the Wiley Online Library or from the author.

## Acknowledgements

B.G.N. thanks Kimberly L. Basset for assistance and discussion about the work carried out with RF Sputtering deposition of LMO. Dr. Lingzi Sang provided very helpful advice about the alkylphosphonate systems and possible methods of characterization of the modified LMO surfaces. This research was supported as a part of the Center for Electrical Energy Science, an Energy Frontier Research Center funded by the U.S. Department of Energy. This work was carried out in part in the Frederick Seitz Materials Research Laboratory Central Facilities. Use of the Center for Nanoscale Materials, an Office of Science user facility, was supported by the U.S. Department of Energy, Office of Science, Office of Basic Energy Sciences, under Contract No. DE-AC02-06CH11357. This research used resources of the Argonne Leadership Computing Facility, which is a DOE Office of Science User Facility supported under Contract No. DE-AC02-06CH11357.

## Conflict of Interest

The authors declare no conflict of interest.

## Keywords

alkylphosphonate, lithium-ion battery cathode, lithium manganese oxide, self-assembled monolayers, surface modification

Received: October 9, 2017
Revised: January 28, 2018
Published online:

[1] J. M. Tarascon, M. Armand, *Nature* **2001**, *414*, 359.
[2] K. Xu, *Chem. Rev.* **2004**, *104*, 4303.
[3] A. Jarry, S. Gottis, Y. S. Yu, J. Roque-Rosell, C. Kim, J. Cabana, J. Kerr, R. Kostecki, *J. Am. Chem. Soc.* **2015**, *137*, 3533.
[4] C. Zhan, J. Lu, A. J. Kropf, T. P. Wu, A. N. Jansen, Y. K. Sun, X. P. Qiu, K. Amine, *Nat. Commun.* **2013**, *4*, 2437.
[5] Y. M. Liu, B. G. Nicolau, J. L. Esbenshade, A. A. Gewirth, *Anal. Chem.* **2016**, *88*, 7171.
[6] B. G. Nicolau, N. Garcia-Rey, B. Dryzhakov, D. D. Dlott, *J. Phys. Chem. C* **2015**, *119*, 10227.
[7] J. L. Esbenshade, A. A. Gewirth, *J. Electrochem. Soc.* **2014**, *161*, A513.
[8] H. W. Ha, N. J. Yun, K. Kim, *Electrochim. Acta* **2007**, *52*, 3236.
[9] J. L. Esbenshade, M. D. Fox, A. A. Gewirth, *J. Electrochem. Soc.* **2015**, *162*, A26.
[10] L. Jaber-Ansari, K. P. Puntambekar, S. Kim, M. Aykol, L. L. Luo, J. S. Wu, B. D. Myers, H. Iddir, J. T. Russell, S. J. Saldana, R. Kumar, M. M. Thackeray, L. A. Curtiss, V. P. Dravid, C. Wolverton, M. C. Hersam, *Adv. Energy Mater.* **2015**, *5*, 1500646.
[11] S. P. Pujari, L. Scheres, A. T. M. Marcelis, H. Zuilhof, *Angew. Chem., Int. Ed.* **2014**, *53*, 6322.
[12] S. A. Paniagua, E. L. Li, S. R. Marder, *Phys. Chem. Chem. Phys.* **2014**, *16*, 2874.
[13] C. Queffelec, M. Petit, P. Janvier, D. A. Knight, B. Bujoli, *Chem. Rev.* **2012**, *112*, 3777.
[14] P. J. Hotchkiss, S. C. Jones, S. A. Paniagua, A. Sharma, B. Kippelen, N. R. Armstrong, S. R. Marder, *Acc. Chem. Res.* **2012**, *45*, 337.
[15] N. Zettsu, S. Kida, S. Uchida, K. Teshima, *Sci. Rep.* **2016**, *6*, 31999.
[16] C. G. Zoski, *Handbook of Electrochemistry*, Elsevier, Amsterdam **2007**.
[17] M. C. Leopold, T. T. Doan, M. J. Mullaney, A. F. Loftus, C. M. Kidd, *J. Appl. Electrochem.* **2015**, *45*, 1069.
[18] K. Hoang, *J. Mater. Chem. A* **2014**, *2*, 18271.
[19] E. Iguchi, Y. Tokuda, H. Nakatsugawa, F. Munakata, *J. Appl. Phys.* **2002**, *91*, 2149.
[20] C. O. Laoire, E. Plichta, M. Hendrickson, S. Mukerjee, K. M. Abraham, *Electrochim. Acta* **2009**, *54*, 6560.
[21] U. K. Sur, V. Lakshminarayanan, *J. Electroanal. Chem.* **2001**, *516*, 31.
[22] V. A. Nikitina, A. V. Rudnev, G. A. Tsirlina, T. Wandlowski, *J. Phys. Chem. C* **2014**, *118*, 15970.
[23] K. Jayanth-Babu, P. Jeevan-Kumar, O. M. Hussain, C. M. Julien, *J. Solid State Electrochem.* **2012**, *16*, 3383.
[24] J. L. Shui, G. S. Jiang, S. Xie, C. H. Chen, *Electrochim. Acta* **2004**, *49*, 2209.
[25] J. P. Schmidt, T. Chrobak, M. Ender, J. Illig, D. Klotz, E. Ivers-Tiffee, *J. Power Sources* **2011**, *196*, 5342.
[26] D. Crain, J. P. Zheng, C. Sulyma, C. Goia, D. Goia, D. Roy, *J. Solid State Electrochem.* **2012**, *16*, 2605.
[27] J.-I. Inamoto, T. Fukutsuka, K. Miyazaki, T. Abe, *ChemistrySelect* **2017**, *2*, 2895.
[28] A. Muthurasu, V. Ganesh, *J. Colloid Interface Sci.* **2012**, *374*, 241.
[29] M. C. Militello, S. W. Gaarenstroom, *Surf. Sci. Spectra* **2001**, *8*, 207.
[30] K. Sato, H. Haruta, Y. Kumashiro, *Phys. Rev. B* **1997**, *55*, 15467.
[31] K. Sato, D. M. Poojary, A. Clearfield, M. Kohno, Y. Inoue, *J. Solid State Chem.* **1997**, *131*, 84.
[32] J. F. Moulder, W. F. Stickle, P. E. Sobol, K. D. Bomben, *PHI-Handbook: Handbook of X-ray Photoelectron Spectroscopy*, Physical Electronics, Eden Prairie, MN **1992**.
[33] E. Hoque, J. A. DeRose, B. Bhushan, K. W. Hipps, *Ultramicroscopy* **2009**, *109*, 1015.
[34] R. T. Haasch, in *Practical Materials Characterization* (Ed: M. Sardela), Springer, New York **2014**, p. 93.
[35] D. Y. Petrovykh, H. Kimura-Suda, L. J. Whitman, M. J. Tarlov, *J. Am. Chem. Soc.* **2003**, *125*, 5219.
[36] S. M. Lane, J. Monot, M. Petit, B. Bujoli, D. R. Talham, *Colloid Surf., B* **2007**, *58*, 34.
[37] S. M. Lane, J. Monot, M. Petit, C. Tellier, B. Bujoli, D. R. Talham, *Langmuir* **2008**, *24*, 7394.
[38] S. A. Paniagua, P. J. Hotchkiss, S. C. Jones, S. R. Marder, A. Mudalige, F. S. Marrikar, J. E. Pemberton, N. R. Armstrong, *J. Phys. Chem. C* **2008**, *112*, 7809.
[39] S. Hofinger, F. Zerbetto, *Chem. Soc. Rev.* **2005**, *34*, 1012.
[40] R. E. Warburton, H. Iddir, L. A. Curtiss, J. Greeley, *ACS Appl. Mater. Interfaces* **2016**, *8*, 11108.
[41] H. Li, P. Paramonov, J. L. Bredas, *J. Mater. Chem.* **2010**, *20*, 2630.
[42] S. A. Paniagua, A. J. Giordano, O. L. Smith, S. Barlow, H. Li, N. R. Armstrong, J. E. Pemberton, J. L. Bredas, D. Ginger, S. R. Marder, *Chem. Rev.* **2016**, *116*, 7117.

 

[43] J. Fischer, C. Adelhelm, T. Bergfeldt, K. Chang, C. Ziebert, H. Leiste, M. Stuber, S. Ulrich, D. Music, B. Hallstedt, H. J. Seifert, *Thin Solid Films* **2013**, *528*, 217.
[44] J. Fischer, D. Music, T. Bergfeldt, C. Ziebert, S. Ulrich, H. J. Seifert, *Thin Solid Films* **2014**, *572*, 208.
[45] P. Verma, P. Maire, P. Novak, *Electrochim. Acta* **2010**, *55*, 6332.
[46] L. A. Huff, J. L. Rapp, J. A. Baughman, P. L. Rinaldi, A. A. Gewirth, *Surf. Sci.* **2015**, *631*, 295.
[47] S. Plimpton, A. Thompson, L. P. Crozier, LAMMPS Molecular Dynamics Simulator, http://lammps.sandia.gov (accessed: February 2017).
[48] S. Nose, M. L. Klein, *Mol. Phys.* **1983**, *50*, 1055.
[49] S. Nose, *J. Chem. Phys.* **1984**, *81*, 511.
[50] W. G. Hoover, *Phys. Rev. A* **1985**, *31*, 1695.
[51] L. Verlet, *Phys. Rev.* **1967**, *159*, 98.
[52] S. A. Petrosyan, A. A. Rigos, T. A. Arias, *J. Phys. Chem. B* **2005**, *109*, 15436.
[53] D. Gunceler, K. Letchworth-Weaver, R. Sundararaman, K. A. Schwarz, T. A. Arias, *Model. Simul. Mater. Sci. Eng.* **2013**, *21*, 074005.
[54] S. L. Dudarev, G. A. Botton, S. Y. Savrasov, C. J. Humphreys, A. P. Sutton, *Phys. Rev. B* **1998**, *57*, 1505.

 